An NGA-West2 Empirical Model for Estimating the Horizontal Spectral Values Generated by Shallow Crustal Earthquakes

I. M. Idriss[a)] **Hon.M.EERI**

An empirical model for estimating the horizontal pseudo-absolute spectral accelerations (PSA) generated by shallow crustal earthquakes was published in 2008 using the recorded earthquake ground motion data collected and documented as part of the original Next Generation Attenuation (NGA) project. A significant number of additional recordings were collected over the past three years, and the 2008 model has been revised using the new data and is presented in this paper. The model was again selected to be simple, and the model parameters were estimated using the expanded database. The revised model incorporates V_{S30} as an independent variable because, with the expanded database, it was found that V_{S30} was required to be included as an independent parameter to allow for a reasonably unbiased fit to the recorded data. It is noted that V_{S30} is not being used to account for nonlinear site response, but strictly to allow for a better fit to the data. These parameters are presented for sites with an average shear wave velocity in the upper 30 m, V_{S30}, for sites with $V_{S30} \geq 450\ \mathrm{m/s}$. Parameters for sites with $V_{S30} < 450\ \mathrm{m/s}$ are not included in this paper. For a site with $V_{S30} = 450\ \mathrm{m/s}$, there is an overall increase in PGA averaging about 50% over a distance of about 100 km using the 2013 model in comparison to the 2008 model. On the other hand, for a site with $V_{S30} = 900\ \mathrm{m/s}$, there is an overall decrease of about 10% using the 2013 model in comparison to the 2008 model. [DOI: 10.1193/070613EQS195M]

INTRODUCTION

As part of the NGA-West2 Project, a flatfile was created containing the information pertaining to 21,539 recordings obtained during earthquakes with magnitudes ranging from 3 to 7.9. The spectral ordinates provided in this flatfile comprised the RotD50 spectral values (5% damping) obtained by rotating the two recorded horizontal components, as described in Boore (2010). Of these recordings, 10,943 were gathered from earthquakes with magnitudes ranging from 4.5 to 7.9, which are considered to be the large-magnitude data set. Removing entries that had no listed magnitude (**M**), mechanism, closest distance to the source (R_{RUP}), average shear wave velocity in the top 30 m, V_{S30}, peak ground acceleration (PGA), peak ground velocity (PGV), peak ground displacement (PGD), and spectral values for $T = 0.01$ s to 20 s, resulted in reducing the number of entries to 10,819. Of these, 6,463 recordings are at free-field sites (Geomatrix first letter designation: A, A-B, B, F, I, I-F, K, L, and M), and

a) Professor emeritus, University of California, Davis; Consulting Geotechnical Engineer, Santa Fe, NM, imidriss@aol.com

Earthquake Spectra, Volume 30, No. 3, pages 1155–1177, August 2014; © 2014, Earthquake Engineering Research Institute

4,097 recordings are at sites where no Geomatrix designation was included in the flatfile. The latter recordings were considered to have been at free-field sites. Thus, the total number of free-field recordings contained in the large-magnitude data set is 10,560.

Examination of the recordings for a number of earthquakes show a significant change in the slope of PGA (and spectral values) versus R_{RUP}, for R_{RUP} exceeding 150 km to 175 km. Accordingly, only recordings obtained at $R_{RUP} \leq 175$ km were selected for this study. In addition, earthquakes having less than three recordings were excluded. The recordings from a number of earthquakes, such as the Taiwan's Smart Array, also were not included. Consequently, the remaining recordings totaled 7,135 and covered the following ranges: **M** 4.5 to **M** 7.9; $R_{RUP} = 0.2$ to 175 km; and $V_{S30} = 100$ m/s to 2,000 m/s.

These 7,135 recordings were generated by 160 earthquakes, which can be summarized as follows: 79 earthquakes in California; 3 in other parts of the United States (Alaska, Idaho, and Nevada); 6 earthquakes in Taiwan (the Chi-Chi main shock and five aftershocks); and 72 earthquakes in Canada, China, Greece, Iran, Italy, Japan, Mexico, New Zealand and Turkey. The full list of these earthquakes is given in the PEER report (Idriss 2013) and is not included in this paper because of length limitations.

EXAMINATION OF THE DATA

Examination of the recorded free-field data (7,135 recordings, as noted above) led to binning the data into three V_{S30} ranges. One bin was for data recorded at sites with $V_{S30} \leq$ 211 m/s ($V_{S30} = 100$ m/s to 211 m/s), which constitute "soft soil sites." The choice of $V_{S30} = 211$ m/s was made to include sites (e.g., El Centro array #7) that are judged to have "soft soil sites" characteristics. Another bin was for data recorded at sites with $V_{S30} \geq$ 450 m/s ($V_{S30} = 450$ m/s to 2,000 m/s). The choice of $V_{S30} = 450$ m/s is based on the considerations discussed later in this paper; these sites may be reasonably designated as "quasi-linear sites" because they appear to show no or very weak nonlinearity, especially for sites with V_{S30} exceeding about 600 m/s (~2,000 fps). The remaining data were recorded at sites with V_{S30} ranging from 211 m/s to 450 m/s; these sites exhibit moderate to strong nonlinear characteristics, especially for sites with V_{S30} less than about 300 m/s (~1,000 fps). The latter sites (V_{S30} ranging from 211 m/s to 450 m/s) can be designated as "nonlinear soil sites."

The number of recordings at "soft soil sites," $V_{S30} \leq 211$ m/s, is 432, of which 51 were recorded during the Chi-Chi, Taiwan, main shock, and 176 were recorded during the five Chi-Chi aftershocks. The number of recordings at "nonlinear soil sites," 211 m/s < V_{S30} < 450 m/s, is 4,158, of which 153 were recorded during the Chi-Chi, Taiwan, main shock, and 558 were recorded during the five Chi-Chi aftershocks. The number of recordings at "quasi-linear sites," $V_{S30} \geq 450$ m/s, is 2,545, of which 192 were recorded during the Chi-Chi, Taiwan, main shock, and 674 were recorded during the five Chi-Chi aftershocks.

The **M** – R_{RUP}, **M** – V_{S30}, **M** – PGA, **M** – PGV, and **M** – PGD distributions of the 7,135 recordings are presented in Figures 1, 2, 3, 4, and 5, respectively. (Note that the spectral values for $T = 0.01$ s are used in this study to represent PGA in lieu of the peak value of the

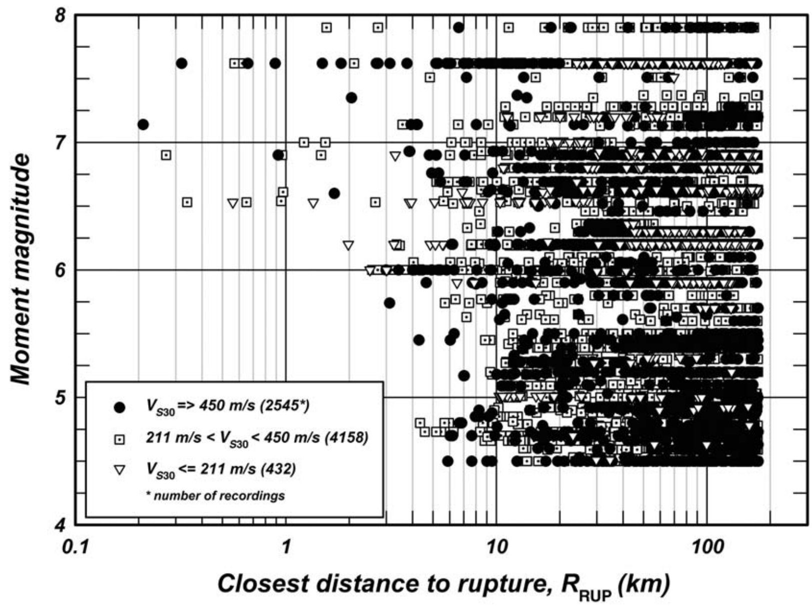

Figure 1. $\mathbf{M} - R_{RUP}$ distribution of NGA-West2 free-field records for distances $\leq$175 km and $\mathbf{M} \geq 4.5$ grouped in three V_{S30} bins ($V_{S30} \geq 450$ m/s; 211 m/s < V_{S30} < 450 m/s; and $V_{S30} \leq 211$ m/s).

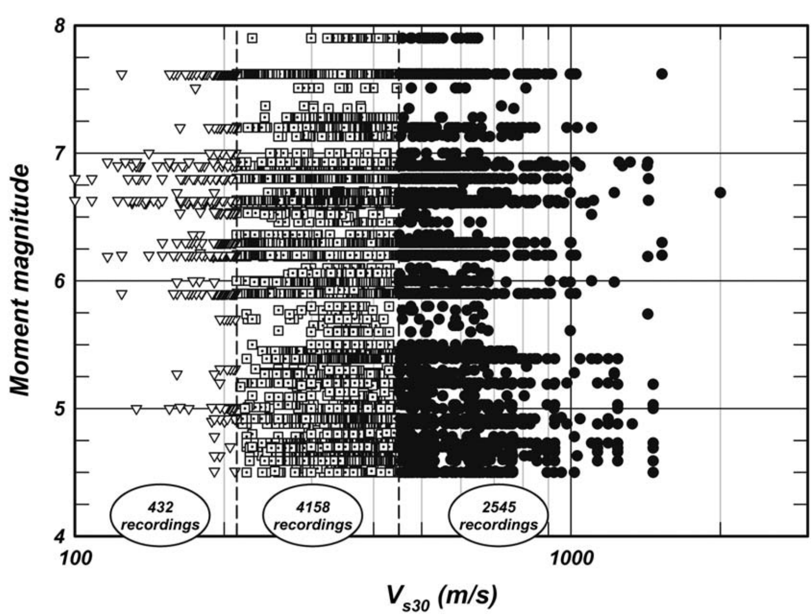

Figure 2. $\mathbf{M} - V_{S30}$ distribution of NGA-West2 free field records for distances $\leq$175 km and $\mathbf{M} \geq 4.5$ grouped in three V_{S30} bins ($V_{S30} \geq 450$ m/s; 211 m/s < V_{S30} < 450 m/s; and $V_{S30} \leq 211$ m/s).

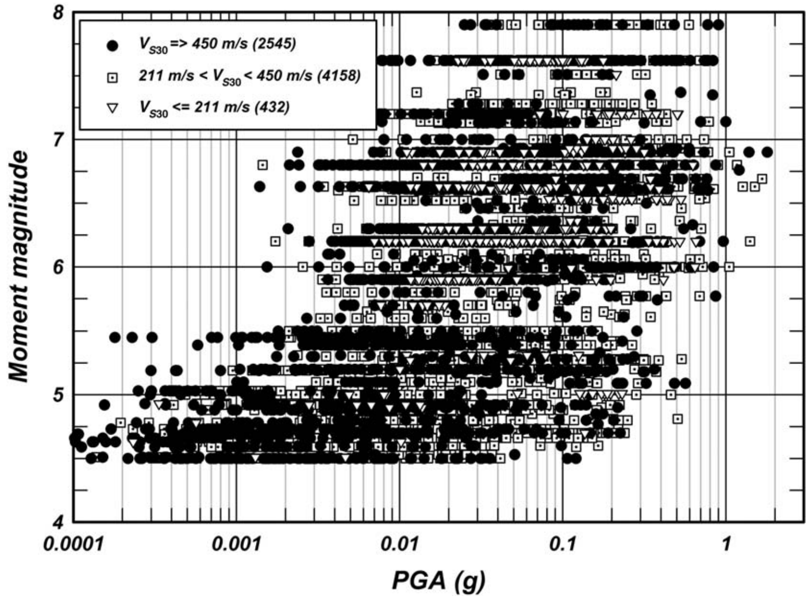

Figure 3. **M** – PGA distribution of NGA-West2 free field records for distances ≤175 km and **M** ≥ 4.5 grouped in three V_{S30} bins ($V_{S30} \geq 450$ m/s; 211 m/s < V_{S30} < 450 m/s; and $V_{S30} \leq 211$ m/s).

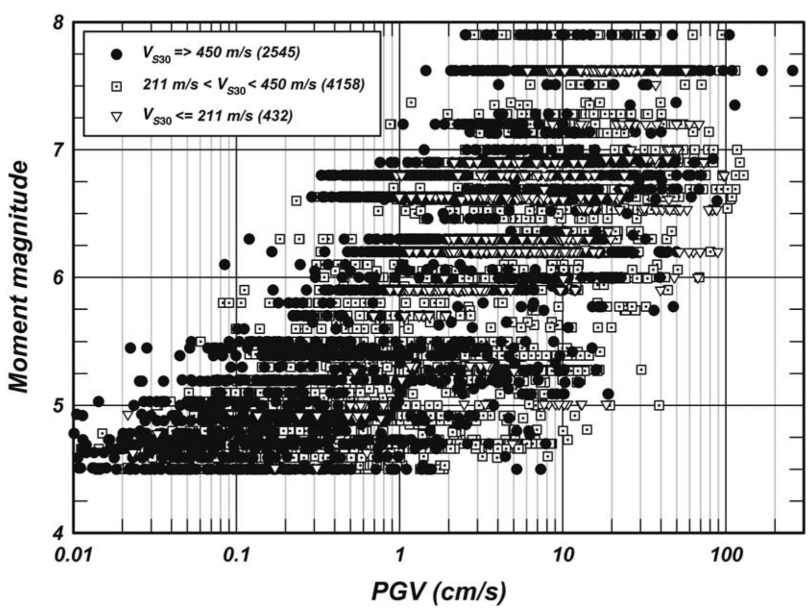

Figure 4. **M** – PGV distribution of NGA-West2 free field records for distances ≤175 km and **M** ≥ 4.5 grouped in three V_{S30} bins ($V_{S30} \geq 450$ m/s; 211 m/s < V_{S30} < 450 m/s; and $V_{S30} \leq 211$ m/s).

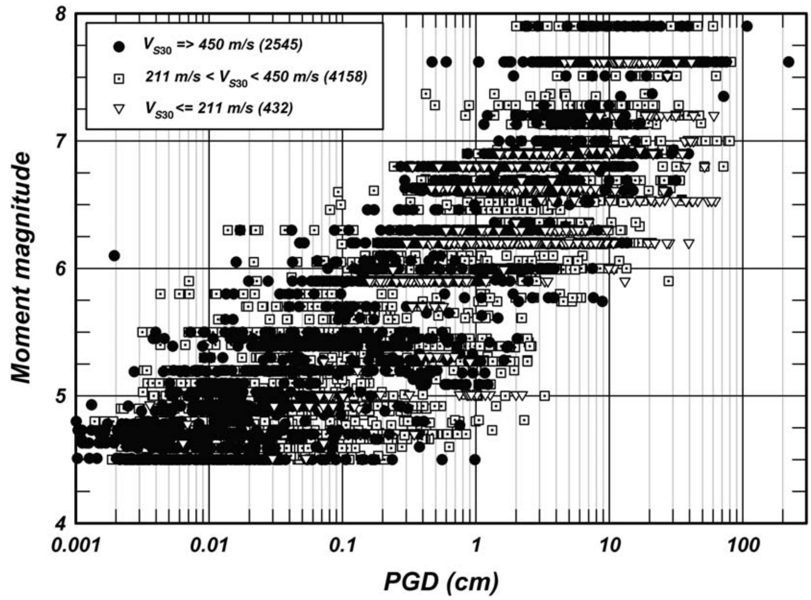

Figure 5. **M** – PGD distribution of NGA-West2 free field records for distances ≤175 km and **M** ≥ 4.5 grouped in three V_{S30} bins ($V_{S30} \geq 450$ m/s; 211 m/s < V_{S30} < 450 m/s; and $V_{S30} \leq 211$ m/s).

rotated accelerogram.) The information gleaned from Figures 1 through 5 is summarized as follows:

Figure 1 (**M** – R_{RUP} distribution) shows that the number of recordings, at distances less than about 10 km, has significantly increased since the first NGA project. However, the recordings within each of the V_{S30} bins, is still not sufficiently robust. It is, therefore, difficult to "mathematically" constrain the values at small distances, particularly for large magnitude earthquakes. Reliance must continue to be placed on some physical attributes, analytical results, and on judgment for constraining the values at small distances.

Figure 2 (**M** – V_{S30} distribution) shows that only a few recordings (65) were at sites with $V_{S30} \geq 1{,}000$ m/s. That is, over 95% of the recordings within the "quasi-linear sites" bin are on stiff or firm soils, and soft or weathered rock.

Figures 3, 4, and 5 (**M** – PGA, **M** – PGV, **M** – PGD distributions, respectively) show that except for a handful of recordings, the values of PGA are less than about 0.8 g, the values of PGV are less than about 100 cm/s, and the values of PGD are less than about 80 cm.

Figures 3, 4, and 5 also show that PGA is far less dependent on magnitude than PGV, and that PGD is somewhat more dependent on magnitude than PGV.

EARTHQUAKE MECHANISM

The flatfile included 7,135 free-field recordings obtained during 160 earthquakes. The mechanism for each earthquake was referenced by a number from 0 to 4 and by a rake angle. The number of free-field recordings for mechanism 0 is 2,659, for mechanism 1 is 39, for mechanism 2 is 2,887, for mechanism 3 is 1,260 and for mechanism 4 is 291.

Earthquakes assigned a mechanism of 0 (e.g., the Denali earthquake) and earthquakes assigned a mechanism of 1 (e.g., the Irpinia earthquake in Italy) were combined as a single group and considered to be representative of strike-slip events. Note that the sense of movement on the Denali fault is strike-slip (USGS 2003) and that on the Irpinia fault is normal (Pantosti et al. 1993). While the initial intent of the NGA project was to develop relationships applicable to normal faults, the recorded data from earthquakes occurring on such faults are too miniscule (39 of the 7,120 free-field recordings, or 0.55%) to constrain such a relationship. Accordingly, until more data are obtained during future normal earthquakes, the parameters included for strike-slip earthquakes in this paper are intended to also be used for estimating spectral ordinates for normal earthquakes.

Earthquakes assigned a mechanism of 2 (e.g., the Northridge earthquake) and earthquakes assigned a mechanism of 3 (e.g., the Loma Prieta earthquake) were combined as a single group and were considered to be representative of reverse events. The flatfile includes recordings from only six earthquakes with mechanism 4. For example, the Anza-02 earthquake, with 72 recordings, is described to have occurred on the San Jacinto fault zone and the earthquake focal mechanism exhibited mixed left-lateral strike-slip and thrust motion on a vertical fault striking N35E (Hauksson et al. 2001). Accordingly, these recordings were also combined with those from the reverse events.

OTHER PARAMETERS

The flatfile included a number of parameters that are not explicitly included in the empirical model used in this paper. The reasons/explanations for not including these parameters are discussed later in this paper.

EXAMINATION OF NONLINEARITY

The recordings examined in the previous section were obtained at sites that encompass a wide range of subsurface conditions. To assess the extent of nonlinearity exhibited at the recording sites, a proxy for "shear strain" induced by the shaking is used. Seismologists have long suggested that the ratio of the peak particle velocity at the ground surface (PGV) divided by the average shear wave velocity of the underlying subsurface profile is a reasonable proxy for the maximum shear strain, γ_{max}, induced during shaking. That is:

$$\gamma_{max} = [PGV/(Avg.V_S)] = (PGV/\bar{V}_S) \tag{1}$$

The use of V_{S30} to represent the average shear wave velocity in this study is dictated by the fact that only that information is available for all the sites under consideration.

To estimate a shear stress–shear strain relationship, PGA can be used as a proxy for shear stress. Accordingly, the values of PGA versus γ_{max} for each of the site bins described above can be readily calculated using the information provided in the flatfile for each recording.

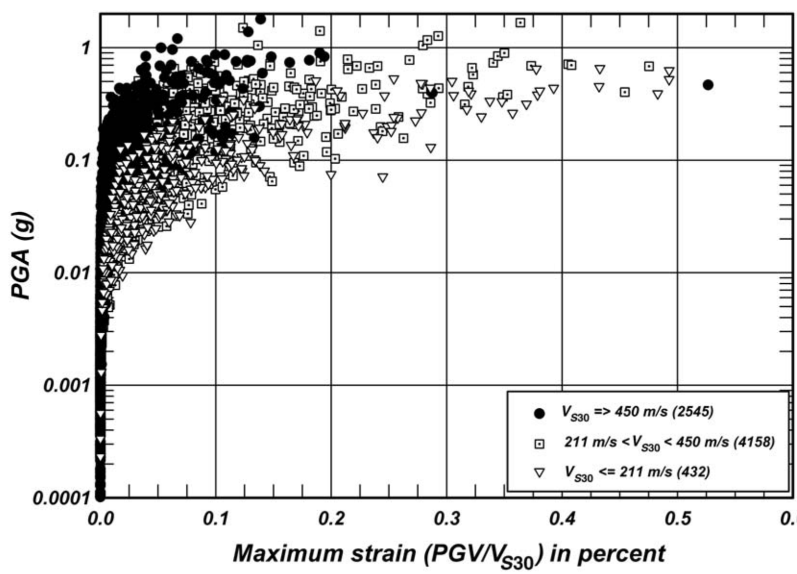

Figure 6. Distribution of maximum strain (PGV/V_{S30}) of NGA-West2 free-field recording stations at distances ≤175 km and $\mathbf{M} \geq 4.5$ grouped in three V_{S30} bins ($V_{S30} \geq 450$ m/s; 211 m/s < V_{S30} < 450 m/s; and $V_{S30} \leq 211$ m/s).

These values are presented in Figure 6, which shows that progressively smaller strains are induced as the "stiffness" of the sites increases and also shows that progressively larger strains are induced for increasing levels of shaking.

The information available for the sites within the "quasi-linear sites" bin ($V_{S30} = 450$ m/s to 2,000 m/s) are examined in more detail in Figure 7. The cumulative distribution of γ_{max} for the recordings obtained during the Chi-Chi, Taiwan, main shock, those obtained during the Chi-Chi, Taiwan, five aftershocks included in the flatfile, and those for all the remaining events within this bin are presented in Figure 7. The information in Figure 7 indicates that the behavior of the sites in Taiwan during the main shock is significantly different from that during the five aftershocks and from that of all the remaining recordings for sites with $V_{S30} = 450$ m/s to 2,000 m/s.

This behavior of the sites from Taiwan can be further explained by the information presented in Figure 8, which shows the values of PGV recorded during the main shock and those recorded during the five aftershocks. Also shown in Figure 8 is the trend of PGV as a function of R_{RUP} based on the values recorded during the main shock and the trend of PGV as a function of R_{RUP} based on the values recorded during aftershocks #3, #5, and #6, whose magnitudes were 6.2, 6.2, and 6.3, respectively. The mechanism for the main shock was 3 and that for aftershocks #3, #5, and #6 was 2; note that the recordings from aftershock #2 (**M** 5.9 and mechanism 2) and aftershock # 4 (**M** 6.2 and mechanism 0) were not included in deriving the trend shown in Figure 8 for aftershocks #3, #5, and #6 because of the smaller magnitude for aftershock #2 and different mechanism for aftershock #4.

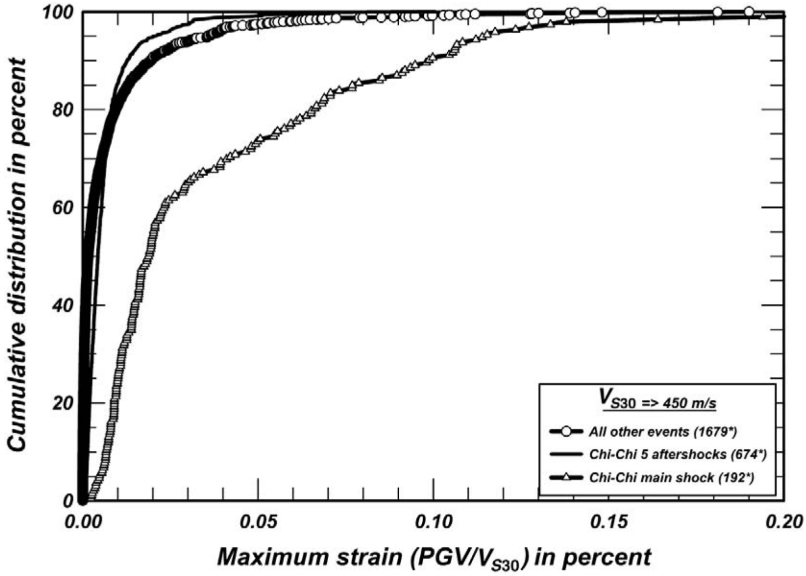

Figure 7. Distribution of maximum strain (PGV/V_{S30}) of NGA-West2 free field recording stations at distances ≤175 km with $V_{S30} \geq 450$ m/s during the Chi-Chi main shock, Chi-Chi aftershocks, and all other earthquakes, $\mathbf{M} \geq 4.5$.

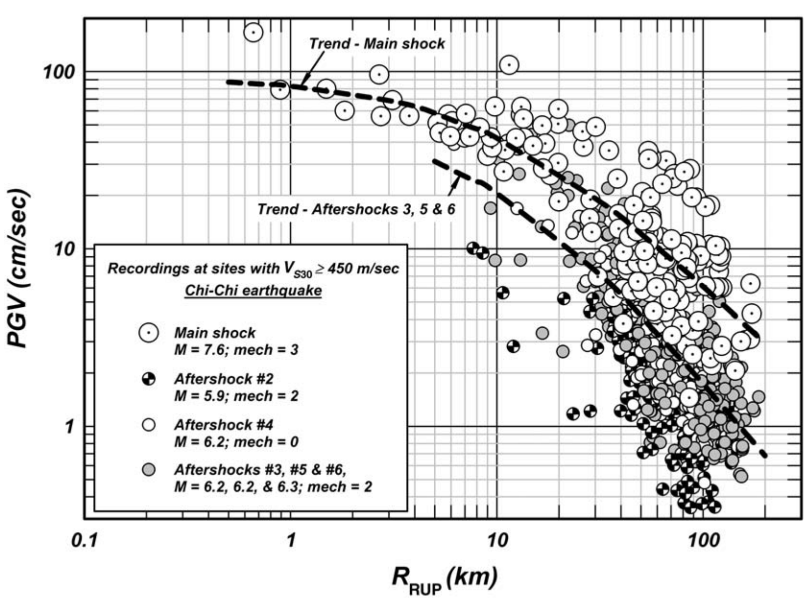

Figure 8. PGV values recorded at sites with $V_{S30} \geq 450$ m/s during the Chi-Chi main shock, and five Chi-Chi aftershocks.

It is readily apparent from the information shown in Figure 8 that, on the average, the values of PGV recorded during the 1999 Chi-Chi main shock are two to four times larger than those recorded during the aftershocks. Obviously this resulted in having much larger values of the proxy γ_{max} for the Chi-Chi main shock than for the aftershocks.

Accordingly, it was judged that the recordings from the 1999 Chi-Chi, Taiwan, main shock should not be included in the $V_{S30} = 450$ m/s to 2,000 m/s bin. However, including the five Chi-Chi aftershocks is appropriate.

Totally different trends were observed for the recordings included in the other two bins in that including or not including the recordings from the Chi-Chi main shock had little effect on the cumulative distribution of γ_{max}. Therefore, the recordings from the Chi-Chi main shock will be included in the "NL soil sites" and the "soft soil sites" bins, when the data in those bins are studied in more detail.

The cumulative distribution of γ_{max} for the recordings within the "quasi-linear sites" bin, (excluding the recordings obtained during the Chi-Chi main shock), those obtained within the "NL soil sites" bin, and those within the "soft soil sites" bin are presented in Figure 9. The information in this figure and the modulus reduction curves shown in Figure 10 lead to the following observations.

The modulus reduction curves shown in Figure 10 cover a wide range of geotechnical materials, from moderately dense sands at relatively shallow depths to competent rock. It is believed that for the "quasi-linear sites" ($V_{S30} = 450$ m/s to 2,000 m/s), probably the most applicable curves are:

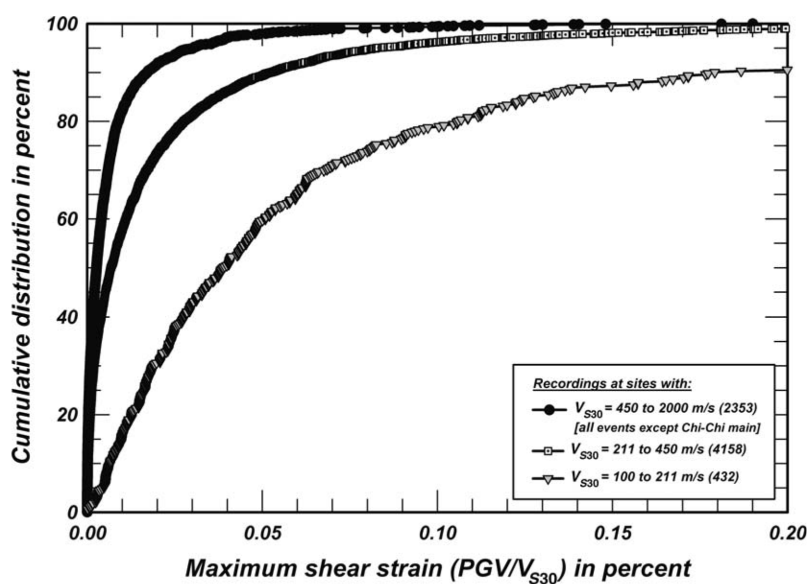

Figure 9. Distribution of maximum strain (PGV/V_{S30}) of NGA-West2 free-field recording stations at distances ≤175 km for the "quasi linear sites" ($V_{S30} = 450$ m/s to 2,000 m/s), the "NL soil sites" ($V_{S30} = 211$ m/s to 450 m/s), and the "soft soil sites" ($V_{S30} = 100$ m/s to 211 m/s).

- A curve very close to that identified as the peninsular range in Figure 10 for sites with V_{S30} ranging from about 450 m/s to 600 m/s.
- The weathered rock curve for sites with V_{S30} ranging from about 600 m/s to 1,000 m/s.
- A curve about halfway between the weathered rock and the competent rock, up to a maximum shear strain of about 0.1%, for sites with $V_{S30} = 1{,}000$ m/s to 2,000 m/s. The remaining "soil" modulus reduction curves in Figure 10 are applicable to the sites with $V_{S30} < 450$ m/s, including the soft soil sites.

The modulus reduction curves in Figure 10 show that for soils (the lower five curves in the figure), the maximum modulus can decrease by about 8% to 16% (average of about 12%) if the strain levels induced by shaking are as high as about 0.01%. In this regard, it should be noted that the shear strains used in Figure 10 represent laboratory-applied shear strains of uniform amplitude over a number of cycles. The shear strains induced by the earthquake ground motions are not uniform in amplitude. The use of an "equivalent uniform strain" to represent the strain level induced during shaking was introduced as part of the equivalent linear site response methodology (Idriss and Seed 1968, Seed and Idriss 1969). The equivalent uniform strain is typically 0.4 to about 0.75 of the maximum shear strain, depending on the duration of shaking, which is a function of magnitude, among others. The following equation has been used for this purpose (Idriss and Sun 1992):

$$\frac{\gamma_{unif}}{\gamma_{max}} = \frac{(\mathbf{M} - 1)}{10} \tag{2}$$

On that basis, and using a ratio of $\gamma_{unif}/\gamma_{max}$ of, say, two thirds, the 0.01% uniform strain would correspond to a maximum strain of 0.015%. At this level of strain, the soil is behaving

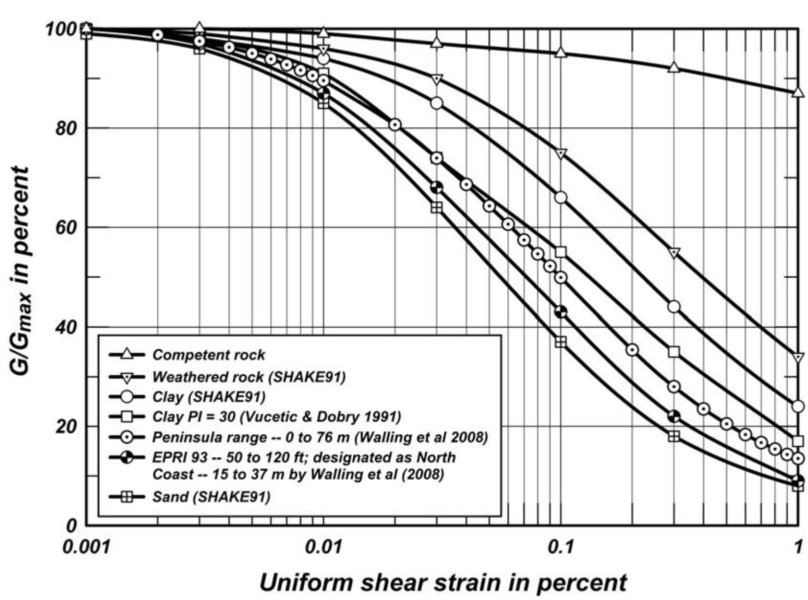

Figure 10. Variations of G/G_{max} with uniform shear strain for various geotechnical materials.

mostly in the linear range with very modest hysteretic loops (i.e., damping) as shaking goes on. Accordingly, a modulus reduction of less than about 12% would constitute essentially a "linear" or "quasi-linear" behavior.

A modulus reduction of 12% corresponds to a uniform shear strain of about 0.01% for soil sites with $V_{S30} < 450$ m/s, as noted above, corresponds to about 0.016% for sites with $V_{S30} = 450$ m/s to 600 m/s, and corresponds to a uniform shear strain about 0.05% to 0.1% for sites with V_{S30} greater than 600 m/s.

Using these uniform shear strain values as the demarcation between essentially linear and nonlinear site response, and, taking into account the conversion from uniform to maximum strain, the cumulative plots in Figure 9 indicate that:

- No more than about 4% of the sites in the "quasi-linear site" bin extended into the mildly nonlinear range.
- At least 30% of the sites in the "NL soil sites" bin extended into the moderately to high nonlinear range.
- Close to 70% of the sites in the "soft soil sites" bin extended well into the nonlinear range.

The recordings at the sites in the "quasi-linear sites" bin are further examined by binning the recording in eight V_{S30} bins ($V_{S30} = 450$ m/s to 800 m/s in 50 m/s increments and one bin for $V_{S30} = 800$ m/s to 2,000 m/s) and by using Equation (2) to obtain the proxy equivalent uniform shear strain for each recording. The corresponding values of PGA versus equivalent uniform shear strain for the eight bins are presented in Figure 11. Using the values noted

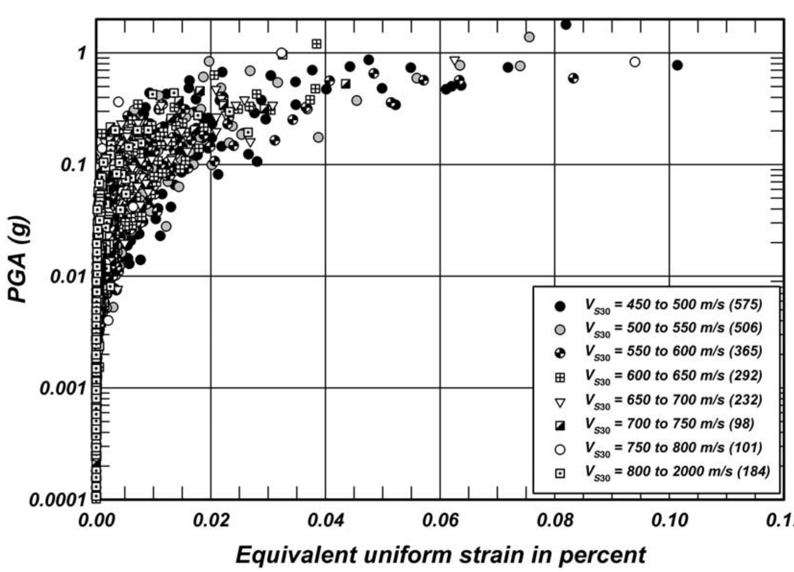

Figure 11. Distribution of equivalent uniform strain of NGA-West2 free-field recording stations with $V_{S30} \geq 450$ m/s at distances ≤175 km and $\mathbf{M} \geq 4.5$ for all earthquakes except Chi-Chi main shock, binned in 50 m/s increments in V_{S30}, from $V_{S30} = 450$ m/s to 800 m/s and for $V_{S30} \geq 800$ m/s.

Table 1. Number of recordings, binned in 50 m/s increments in V_{S30} from $V_{S30} = 450$ m/s to 800 m/s and for $V_{S30} \geq 800$ m/s, and number of recordings at sites, within each V_{S30} bin, where response can be considered nonlinear (NL)

Range of V_{S30} within the bin	Number of recordings within bin	NL sites**	Percent NL
450 m/s to 500 m/s	575	30	5.2
500 m/s to 550 m/s	506	20	4.0
550 m/s to 600 m/s	365	16	4.4
600 m/s to 650 m/s	292	0	0
650 m/s to 700 m/s	232	1	0.4
700 m/s to 750 m/s	98	0	0
750 m/s to 800 m/s	101	0	0
800 m/s to 2,000 m/s	184	0	0
All recordings* 450 m/s to 2,000 m/s	2,353	67	2.9

*NGA-West2 free field recording stations with $V_{S30} \geq 450$ m/s at distances ≤175 km and $\mathbf{M} \geq 4.5$ for all earthquakes except Chi-Chi main shock.
**Number of recordings at sites where response can be considered nonlinear (NL).

above for demarcation of linear-nonlinear behavior and the information in Figure 11 produces the results listed in Table 1.

The data in the other two V_{S30} bins will be examined in more detail in separate reports. Such examinations will incorporate the results of prior studies, such as those completed by Choi and Stewart (2005), Walling et al. (2008), and Kamai et al. (2012).

EMPIRICAL MODEL

BASIC FORM

Based on the considerations summarized earlier in this paper, an empirical model for estimating the average horizontal values of PSA (5% spectral damping) is developed using only the recordings described above as being part of the quasi-linear sites V_{S30} bin (i.e., $V_{S30} = 450$ m/s to 2,000 m/s). These recordings, totaling 2353, were obtained during 151 earthquakes—74 of which occurred in California, 1 in Nevada, 1 in Idaho, the 5 aftershocks after the 1999 Chi-Chi earthquake in Taiwan, 5 in Japan, the Wenchuan main shock and its 54 aftershocks in China, 2 in New Zealand, and 15 in other countries (Canada, Mexico, Italy, Turkey, and Iran). These earthquakes are listed in the recently published PEER report (Idriss 2013) and are not included in this paper because of print space limitations.

The general form of the model adopted in this study is as follow:

$$Ln[PSA] = \alpha_1 + \alpha_2\mathbf{M} + \alpha_3(8.5 - \mathbf{M})^2 - [\beta_1 + \beta_2\mathbf{M}]Ln(R_{RUP} + 10) + \xi Ln(V_{S30}) + \gamma R_{RUP} + \varphi F \tag{3}$$

The variables included in Equation 3 are defined as follows: PSA in g is the 5% damped pseudo-absolute spectral acceleration; **M** is moment magnitude; R_{RUP} in km is the closest distance to the rupture surface; V_{S30} in m/s is the average shear wave velocity over the top 30 m below the ground surface; and F refers to source mechanism, with $F = 0$ referring to strike-slip and normal mechanisms and $F = 1$ referring to reverse and oblique mechanisms. Note that the reverse mechanism database used in this study includes all data from events with mechanism equal to 2, 3, and 4, and all strike-slip mechanism database includes all data from events with mechanism 0 and 1. The dearth of data for mechanism 1 (normal faulting) precluded separating its data from the strike-slip database. The regression coefficients (α_1, α_2, α_3, β_1, β_2, ξ, γ, and φ) were determined from the regression results.

REGRESSION COEFFICIENTS

The coefficients derived are listed in Table 2 for $\mathbf{M} \leq 6.75$ and in Table 3 for $\mathbf{M} \geq 6.75$. Note that for $V_{S30} > 1{,}200$ m/s, the PSA values calculated using $V_{S30} = 1{,}200$ m/s are used. The reason for the latter statement is that there are only 34 recordings at sites with $V_{S30} > 1{,}200$ m/s, consisting of 15 recordings at sites with V_{S30} ranging from about 1,220 to 1,270 m/s, 2 at sites with V_{S30} equal to about 1,320 m/s, 13 at sites with V_{S30}

Table 2. Derived coefficients for sites with $V_{S30} \geq 450$ m/s and $\mathbf{M} \leq 6.75$

Period (s)	α_1	α_2	α_3	β_1	β_2	ξ	γ	φ
0.01	7.0887	0.2058	0.0589	2.9935	−0.2287	−0.854	−0.0027	0.08
0.02	7.1157	0.2058	0.0589	2.9935	−0.2287	−0.854	−0.0027	0.08
0.03	7.2087	0.2058	0.0589	2.9935	−0.2287	−0.854	−0.0027	0.08
0.04	7.3287	0.2058	0.0589	2.9935	−0.2287	−0.854	−0.0027	0.08
0.05	6.2638	0.0625	0.0417	2.8664	−0.2418	−0.631	−0.0061	0.08
0.075	5.9051	0.1128	0.0527	2.9406	−0.2513	−0.591	−0.0056	0.08
0.1	7.5791	0.0848	0.0442	3.0190	−0.2516	−0.757	−0.0042	0.08
0.15	8.0190	0.1713	0.0329	2.7871	−0.2236	−0.911	−0.0046	0.08
0.2	9.2812	0.1041	0.0188	2.8611	−0.2229	−0.998	−0.0030	0.08
0.25	9.5804	0.0875	0.0095	2.8289	−0.2200	−1.042	−0.0028	0.08
0.3	9.8912	0.0003	−0.0039	2.8423	−0.2284	−1.030	−0.0029	0.08
0.4	9.5342	0.0027	−0.0133	2.8300	−0.2318	−1.019	−0.0028	0.08
0.5	9.2142	0.0399	−0.0224	2.8560	−0.2337	−1.023	−0.0021	0.08
0.75	8.3517	0.0689	−0.0267	2.7544	−0.2392	−1.056	−0.0029	0.08
1	7.0453	0.1600	−0.0198	2.7339	−0.2398	−1.009	−0.0032	0.06
1.5	5.1307	0.2429	−0.0367	2.6800	−0.2417	−0.898	−0.0033	0.04
2	3.3610	0.3966	−0.0291	2.6837	−0.2450	−0.851	−0.0032	0.02
3	0.1784	0.7560	−0.0214	2.6907	−0.2389	−0.761	−0.0031	0.02
4	−2.4301	0.9283	−0.0240	2.5782	−0.2514	−0.675	−0.0051	0
5	−4.3570	1.1209	−0.0202	2.5468	−0.2541	−0.629	−0.0059	0
7.5	−7.8275	1.4016	−0.0219	2.4478	−0.2593	−0.531	−0.0057	0
10	−9.2857	1.5574	−0.0035	2.3922	−0.2586	−0.586	−0.0061	0

Note that for $V_{S30} > 1{,}200$ m/s, the PSA values calculated using $V_{S30} = 1{,}200$ m/s are used.

Table 3. Derived coefficients for sites with $V_{S30} \geq 450$ m/s and $\mathbf{M} \geq 6.75$

Period (s)	α_1	α_2	α_3	β_1	β_2	ξ	γ	φ
0.01	9.0138	−0.0794	0.0589	2.9935	−0.2287	−0.854	−0.0027	0.08
0.02	9.0408	−0.0794	0.0589	2.9935	−0.2287	−0.854	−0.0027	0.08
0.03	9.1338	−0.0794	0.0589	2.9935	−0.2287	−0.854	−0.0027	0.08
0.04	9.2538	−0.0794	0.0589	2.9935	−0.2287	−0.854	−0.0027	0.08
0.05	7.9837	−0.1923	0.0417	2.7995	−0.2319	−0.631	−0.0061	0.08
0.075	7.7560	−0.1614	0.0527	2.8143	−0.2326	−0.591	−0.0056	0.08
0.1	9.4252	−0.1887	0.0442	2.8131	−0.2211	−0.757	−0.0042	0.08
0.15	9.6242	−0.0665	0.0329	2.4091	−0.1676	−0.911	−0.0046	0.08
0.2	11.1300	−0.1698	0.0188	2.4938	−0.1685	−0.998	−0.0030	0.08
0.25	11.3629	−0.1766	0.0095	2.3773	−0.1531	−1.042	−0.0028	0.08
0.3	11.7818	−0.2798	−0.0039	2.3772	−0.1595	−1.030	−0.0029	0.08
0.4	11.6097	−0.3048	−0.0133	2.3413	−0.1594	−1.019	−0.0028	0.08
0.5	11.4484	−0.2911	−0.0224	2.3477	−0.1584	−1.023	−0.0021	0.08
0.75	10.9065	−0.3097	−0.0267	2.2042	−0.1577	−1.056	−0.0029	0.08
1	9.8565	−0.2565	−0.0198	2.1493	−0.1532	−1.009	−0.0032	0.06
1.5	8.3363	−0.2320	−0.0367	2.0408	−0.1470	−0.898	−0.0033	0.04
2	6.8656	−0.1226	−0.0291	2.0013	−0.1439	−0.851	−0.0032	0.02
3	4.1178	0.1724	−0.0214	1.9408	−0.1278	−0.761	−0.0031	0.02
4	1.8102	0.3001	−0.0240	1.7763	−0.1326	−0.675	−0.0051	0
5	0.0977	0.4609	−0.0202	1.7030	−0.1291	−0.629	−0.0059	0
7.5	−3.0563	0.6948	−0.0219	1.5212	−0.1220	−0.531	−0.0057	0
10	−4.4387	0.8393	−0.0035	1.4195	−0.1145	−0.586	−0.0061	0

Note that for $V_{S30} > 1{,}200$ m/s, the PSA values calculated using $V_{S30} = 1{,}200$ m/s are used.

ranging from about 1,420 to 1,460 m/s, 3 at sites with $V_{S30} = 1{,}525$ m/s, and one at a site with $V_{S30} = 2{,}000$ m/s. Thus, the number of recordings at sites with $V_{S30} > 1{,}200$ m/s is very small and 28 of the 34 recordings are clustered around two relatively narrow ranges of V_{S30}. After a number of trials, it was concluded that: (a) the recordings at sites with $V_{S30} >$ 1,200 m/s have practically no influence on the regression results; and (b) the smallest average residual over the range of $V_{S30} = 1{,}220$ to 1,525 m/s is obtained when the PSA values calculated using $V_{S30} = 1{,}200$ m/s are used for sites with $V_{S30} > 1{,}200$ m/s.

STANDARD ERROR TERMS

The standard error (SE) terms were obtained as part of the regression analyses and were fitted to the following expression for ease of use:

$$SE = 1.18 + 0.035Ln(T) - 0.06\mathbf{M} \tag{4}$$

Equation 4 shows a small dependence of the SE term on magnitude, which is obtained by minimizing the standardized residuals. The value of SE for $\mathbf{M} < 5$ is assumed equal to that for $\mathbf{M}$ 5. The minimum value of SE is assumed equal to that for $\mathbf{M}$ 7.5. Also, the values of SE at $T < 0.05$ s is kept equal to that at $T = 0.05$ s and that at $T > 3$ s, SE is kept equal to that at $T = 3$ s.

RESIDUALS

The residuals for PGA (i.e., $T = 0.01$ s) are plotted in Figure 12 in terms of residuals versus magnitude, residuals versus distance, and residuals versus V_{S30}. The corresponding residuals for $T = 0.2$ s and for $T = 1$ s are presented in Figures 13 and 14, respectively. The

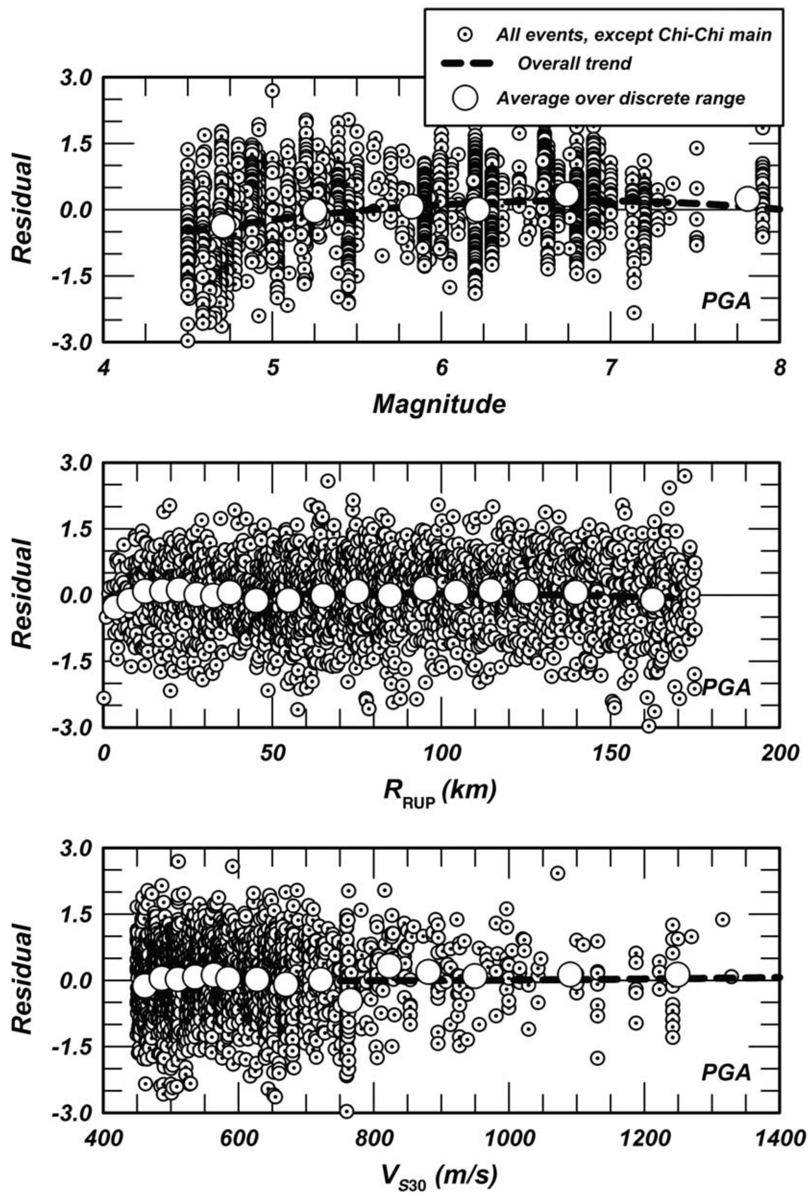

Figure 12. Residuals versus magnitude, rupture distance and V_{S30} using the derived equation for estimating PGA at sites with $V_{S30} \geq 450$ m/s.

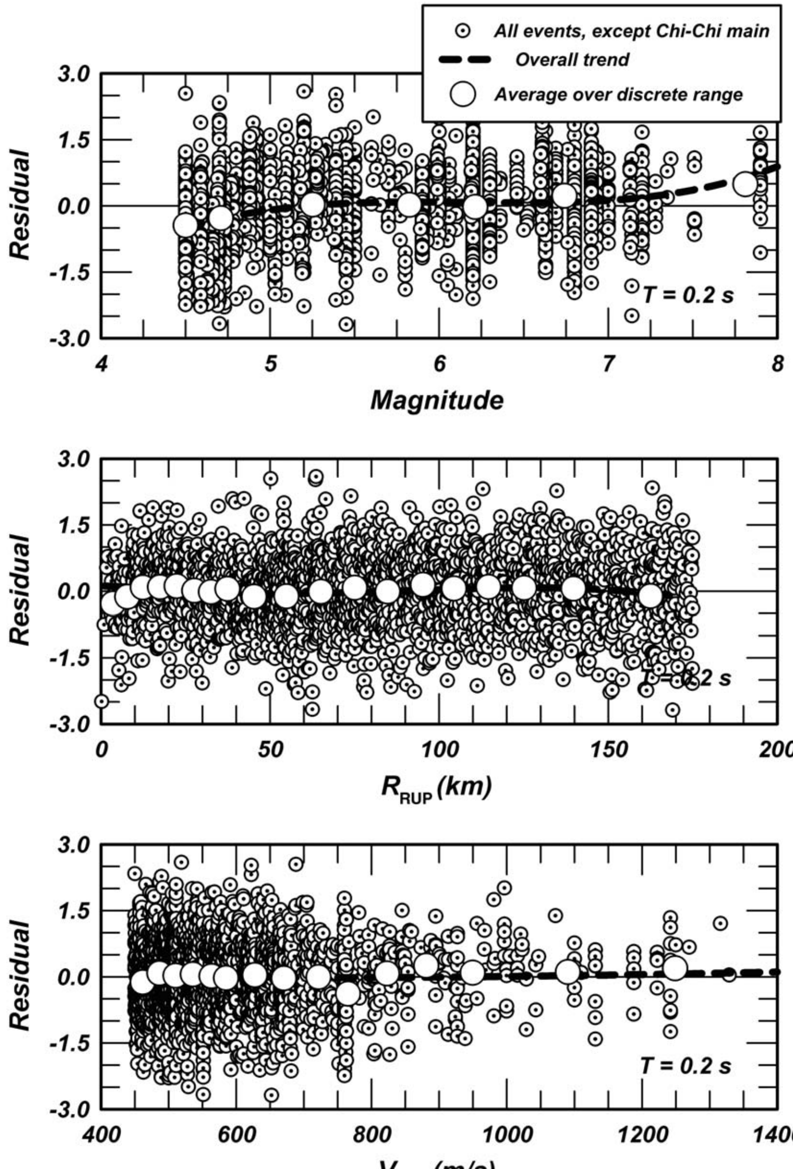

Figure 13. Residuals versus magnitude, rupture distance and V_{S30} using the derived equation for estimating PSA for $T = 0.2$ s at sites with $V_{S30} \geq 450$ m/s.

results in these figures indicate that the fitted parameters provide a very good representation of the data in the magnitude range of 5.2 to 7.9 for PGA, 5.2 to 7.3 for $T = 0.2$ s, and 5.2 to 7.5 for $T = 1$ s. The results also indicate that good representation is obtained for PGA, $T = 0.2$ s and $T = 1$ s essentially in the entire distance and V_{S30} ranges.

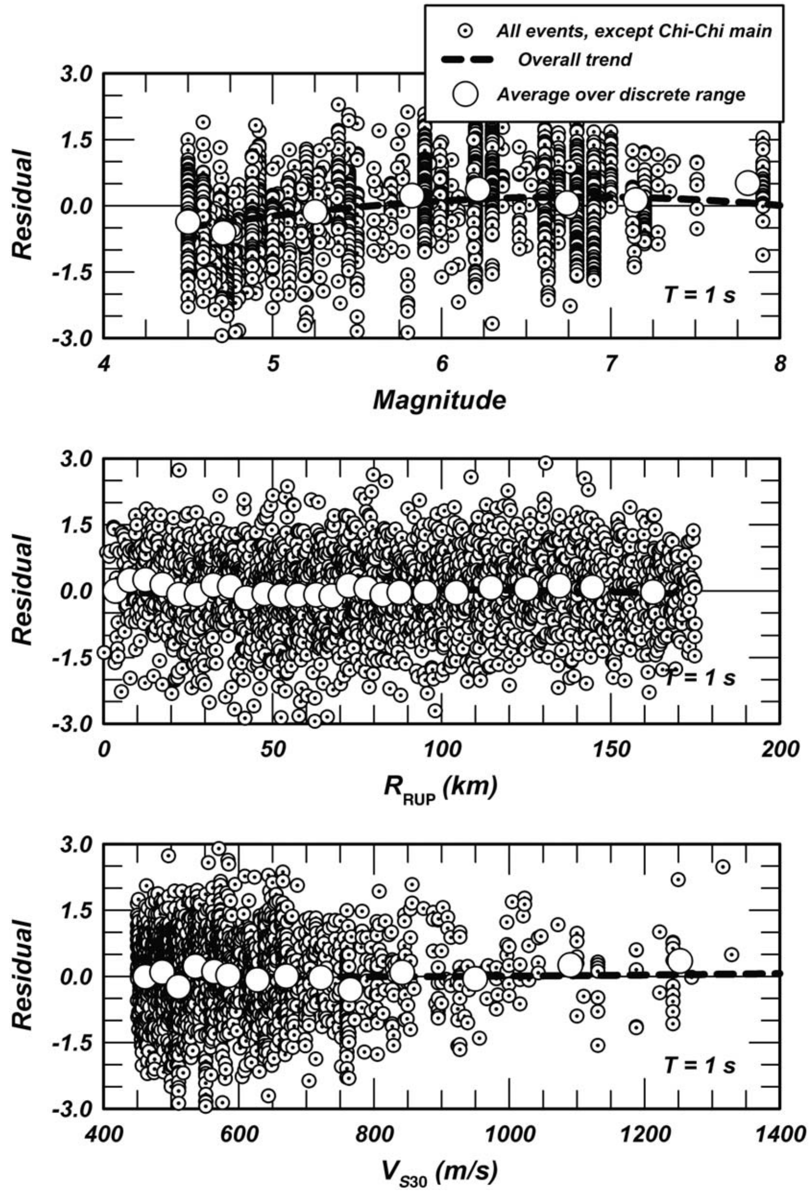

Figure 14. Residuals versus magnitude, rupture distance and V_{S30} using the derived equation for estimating PSA for $T = 1$ s at sites with $V_{S30} \geq 450$ m/s.

COMPARISONS WITH 2008 NGA ATTENUATION RELATIONSHIPS

The median values of PGA as a function of R_{RUP} for $\mathbf{M} = 7$, $V_{S30} = 450$ m/s, and $V_{S30} = 900$ m/s, calculated using the coefficients in Table 3, are presented in Figure 15 considering a strike-slip event (mechanism 0). Also shown in Figure 15 are the median values

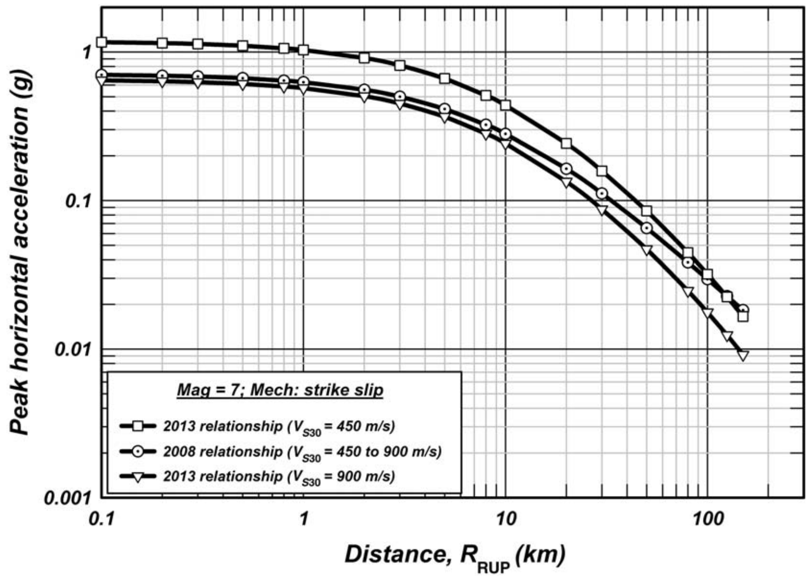

Figure 15. PGA versus R_{RUP} for $\mathbf{M} = 7$ occurring on a strike-slip source calculated using the coefficients derived for the 2008 model ($V_{S30} = 450$ to 900 m/s) and the coefficients derived for the 2013 model for $V_{S30} = 450$ m/s and for $V_{S30} = 900$ m/s.

of PGA as a function of R_{RUP} for $\mathbf{M} = 7$ using the coefficients developed for the author's 2008 model (Idriss 2008). The coefficients for the 2008 model were found, based on the then-available data for sites with $V_{S30} = 450$ m/s to 900 m/s, to be independent of V_{S30}. The 2013 model includes V_{S30} as an independent variable (see Equation 3). The results shown in Figure 15 highlight the effects of V_{S30} on PGA. For a site with $V_{S30} = 450$ m/s, there is an overall increase in PGA averaging about 50% over a distance of about 100 km using the 2013 model in comparison to the 2008 model. On the other hand, for a site with $V_{S30} = 900$ m/s there is an overall decrease of about 10% using the 2013 model in comparison to the 2008 model. Comparable observations are obtained for changes in PSA for almost all periods considered.

OTHER PARAMETERS

As noted earlier, the flatfile included a number of parameters, such as: depth to the top of rupture, Z_{TOR}; dip angle in degrees; horizontal distance to the surface projection of the top of rupture, R_x; closest distance to the surface projection of the rupture surface, designated Joyner-Boore distance, or R_{JB}; sediment (or basin) thickness in terms of depth to shear wave velocities of 1.0 km/s, 1.5 km/s, and 2.5 km/s (designated $Z_{1.0}$, $Z_{1.5}$, and $Z_{2.5}$, respectively); and location relative to hanging wall/foot wall, as appropriate. These parameters are not explicitly included in the empirical model used in this paper; the reasons/explanations for not including these parameters are discussed below:

The depth to the top of rupture, Z_{TOR}, is not included because this parameter does not seem to bias the results for sites with $V_{S30} \geq 450$ m/s, for Z_{TOR} less than about 13 km, as shown in Figures 16 and 17. Figure 16 shows the residuals versus depth to the top of rupture, Z_{TOR}, using the derived equation for estimating PGA at sites with $V_{S30} \geq 450$ m/s; the figure also shows the trend of the residuals for $Z_{TOR} \leq 13$ km. The corresponding values for estimating PSA for $T = 1$ s are presented in Figure 17.

The dip angle, δ, is not included because this parameter does not seem to bias the results for sites with $V_{S30} \geq 450$ m/s, for $24° < \delta \leq 90°$, as shown in Figures 18 and 19. Figure 18 shows the residuals versus dip angle, δ, using the derived equation for estimating PGA at sites with $V_{S30} \geq 450$ m/s; the figure also shows the trend of the residuals for $24° < \delta \leq 90°$. The corresponding values for estimating PSA for $T = 1$ s are presented in Figure 19.

Neither the horizontal distance to the surface projection of the top of rupture, R_x, nor the closest distance to the surface projection of the rupture surface (i.e., R_{JB},) is included. For a given set of dip angle and R_{RUP}, the values of R_x and R_{JB} can readily be calculated and hence neither parameter needs to be included in the model as an independent parameter for sites with $V_{S30} \geq 450$ m/s.

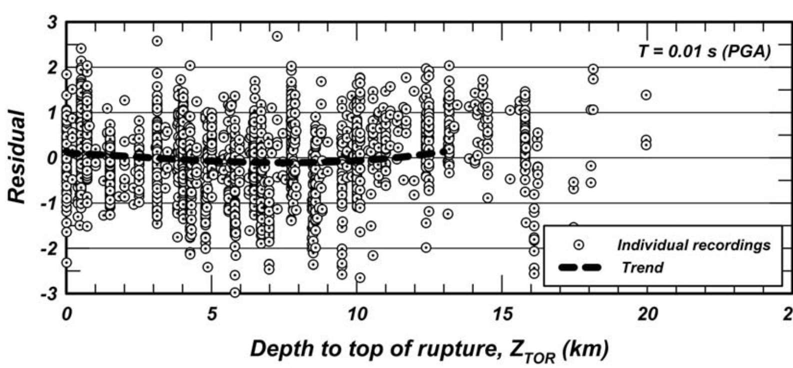

Figure 16. Residuals versus depth to the top of rupture, Z_{TOR}, using the derived equation for estimating PGA at sites with $V_{S30} \geq 450$ m/s.

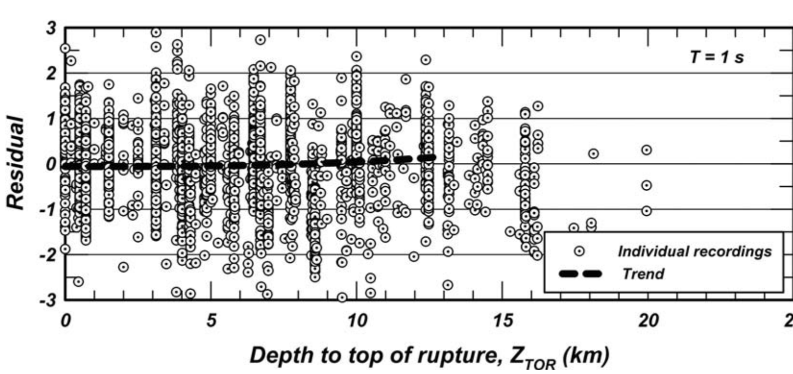

Figure 17. Residuals versus depth to the top of rupture, Z_{TOR}, using the derived equation for estimating PSA for $T = 1$ s at sites with $V_{S30} \geq 450$ m/s.

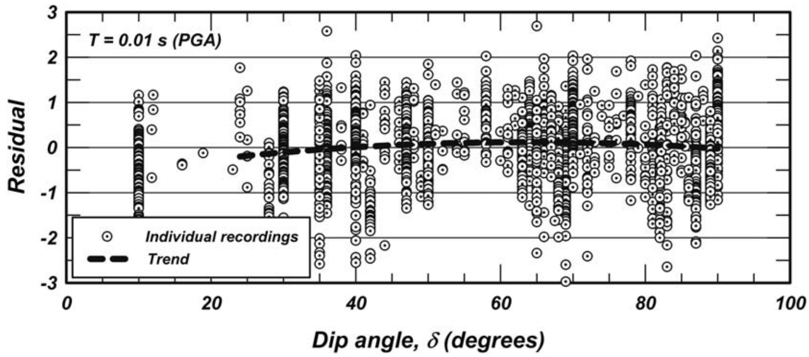

Figure 18. Residuals versus dip angle, δ, using the derived equation for estimating PGA at sites with $V_{S30} \geq 450$ m/s.

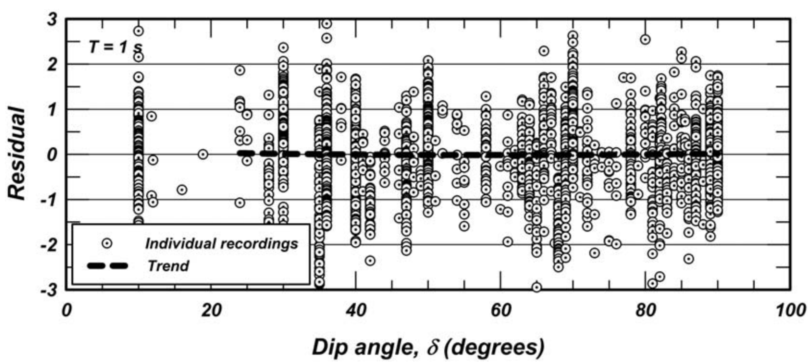

Figure 19. Residuals versus dip angle, δ, using the derived equation for estimating PSA for $T = 1$ s at sites with $V_{S30} \geq 450$ m/s.

The sediment (or basin) thickness in terms of depth to shear wave velocities of 1.0 km/s, 1.5 km/s, and 2.5 km/s (designated $Z_{1.0}$, $Z_{1.5}$, and $Z_{2.5}$ in the flatfile, respectively) were not included in the model. For the 2353 recordings at sites with $V_{S30} \geq 450$ m/s, the flatfile listed only 1,421, 345, and 1,314 values for the parameters $Z_{1.0}$, $Z_{1.5}$, and $Z_{2.5}$, respectively. The number of recordings for which values of $Z_{1.0}$ and $Z_{2.5}$ are available for these sites is reasonably sufficient to examine bias with respect to these two parameters when they are excluded from the model. On the other hand, the number of recordings for which values of $Z_{1.5}$ are available for these sites is inadequate and, therefore, $Z_{1.5}$ is not considered any further.

As shown in Figures 20 and 21, there seems to be practically no dependence of PGA on $Z_{1.0}$ for $Z_{1.0}$ less than about 200 m and little dependence in the range of $Z_{1.0}$ from 200 to 400 m; only 149 points (out of 1,421) that are at $Z_{1.0}$ deeper than 400 m. Similar trends were obtained for the dependence of PSA at $T = 1$ s on $Z_{1.0}$ and dependence of PGA and PSA at

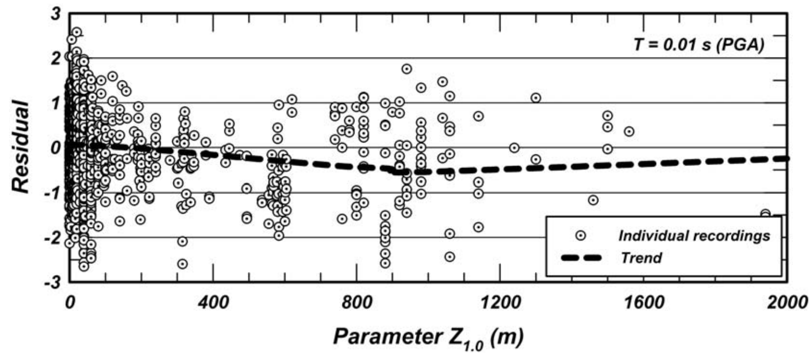

Figure 20. Residuals versus parameter $Z_{1.0}$ (for the full $Z_{1.0}$ range, 0 m to 1,940 m) using the derived equation for estimating PGA at sites with $V_{S30} \geq 450$ m/s.

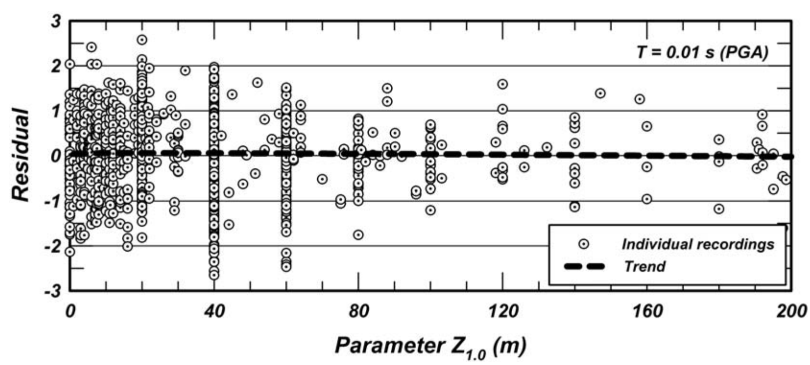

Figure 21. Residuals versus parameter $Z_{1.0}$ (for $Z_{1.0} \leq 200$ m) using the derived equation for estimating PGA at sites with $V_{S30} \geq 450$ m/s.

$T = 1$ s on $Z_{2.5}$. Accordingly, neither parameter was included as an independent parameter in the model for sites with $V_{S30} \geq 450$ m/s.

The number of recordings designated in the flatfile as being on the hanging wall (HW) is only 95 out of the 2,353 recordings used in deriving the model for sites with $V_{S30} \geq 450$ m/s. Therefore, this miniscule number is totally inadequate to constrain the effects of hanging wall for the empirically based model for these sites.

CONCLUDING REMARKS

The recorded motions collected and documented as part of the NGA West2 project covered a wide range of earthquake magnitude (**M** 3 to **M** 7.9), a wide range of distances (less than 1 km to over 1,500 km) and a wide range of site conditions as represented by V_{S30} (100 m/s to 2,100 m/s). The recorded data for $\mathbf{M} \geq 4.5$, which may be considered as the large magnitude data set, were segregated into three V_{S30} bins. An empirical model for estimating the average horizontal values of pseudo-absolute spectral accelerations (PSA) generated by crustal earthquakes has been developed for sites in the bin with $V_{S30} \geq 450$ m/s, designated as the "quasi-linear sites". The fitted coefficients, listed in Tables 2 and 3, provide a reasonable to excellent representation of the data in the magnitude range of about 5 to 8 and excellent representation essentially in the entire distance and V_{S30} ranges.

The model used by the author in 2008 did not include V_{S30} as an independent variable because for the range of sites considered in that model (sites with V_{S30} ranging from 450 m/s to 900 m/s and for sites with $V_{S30} > 900$ m/s), the derived values of PSA did not seem to be dependent on V_{S30}. The model presented in this paper, however, incorporates V_{S30} as an independent variable because, with the expanded database (829 to 2,353 recordings), it was found that V_{S30} was required to be included as an independent parameter to allow for a reasonably unbiased fit to the recorded data. It is noted that V_{S30} is not being used to account for nonlinear site response, but strictly to allow for a better fit to the data.

The use of this model should be limited to $\mathbf{M} \geq 5$, to distances less than about 150 km, and to $V_{S30} \geq 450$ m/s. For sites with $V_{S30} > 1{,}200$ m/s, the PSA values calculated using $V_{S30} = 1{,}200$ m/s are used.

ACKNOWLEDGEMENTS

This project was sponsored by PEER's Program of Applied Earthquake Engineering Research of Lifeline Systems supported by the California Energy Commission, California Department of Transportation, and the Pacific Gas & Electric Company. The author is grateful for the support provided by this program. The author's interactions with the other NGA developers—Drs. N. Abrahamson, G. Atkinson, D. Boore, Y. Bozorgnia, K. Campbell, B. Chiou, R. Kamai, E. Seyhan, W. Silva, J. Stewart, and R. Youngs—have been most invigorating and intellectually satisfying.

The author is grateful to the many young post-doctoral fellows at PEER, without whose input, efforts, and enthusiasm the NGA-West2 Project would have been far more difficult to complete. While each of these post-docs contributed significantly to this effort, three particularly stand out, namely, Dr. Timothy Ancheta, Dr. Albert Kottke, and Dr. Tadahiro Kishida. Dr. Yousef Bozorgnia, Executive Director of PEER, was instrumental in managing the project. All this support is gratefully acknowledged. Finally, the author appreciates the comments offered by three anonymous reviewers and believes that responding to their comments improved the paper.

REFERENCES

Boore, D. M., 2010. Orientation-independent, nongeometric-mean measures of seismic intensity from two horizontal components of motion, *Bull. Seismol. Soc. Am.* **100**, 1830–1835.

Choi, Y., and Stewart, J. P., 2005. Nonlinear site amplification as function of 30 m shear wave velocity, *Earthquake Spectra* **21**, 1–30.

Hauksson, E., Hutton, K., Jones, L., and Given, D., 2001. *M5.1 Anza Earthquake of October 30, 2001*, Preliminary Report from the Southern California Seismic Network/TriNet, available at http://pasadena.wr.usgs.gov/eqinthenews/ci9718013/reports/2.html.

Idriss, I. M., and Seed, H. B., 1968. Seismic response of horizontal soil layers, *J.Soil Mech. Foundations Div., ASCE* **94**, 1003–1031.

Idriss, I. M., and Sun, J., 1992. *User's Manual for SHAKE91: A Computer Program for Conducting Equivalent Linear Seismic Response Analyses of Horizontally Layered Soil Deposits*, Center for Geotechnical Modeling, Department of Civil and Environment Engineering, University of California, Davis, CA.

Idriss, I. M., 2008. An NGA empirical model for estimating the horizontal spectral values generated by shallow crustal earthquakes, *Earthquake Spectra* **24**, 217–242.

Kamai, R., Abrahamson, N. A., and Silva, W. J., 2013. *Nonlinear Horizontal Site Response for the NGA-West2 Project*, PEER Report No. 2013/12, Pacific Earthquake Engineering Research Center, University of California, Berkeley, CA, 69 pp.

Pantosti, D., Schwartz, D. P., and Valensise, G., 1993. Paleo-seismology along the 1980 surface rupture of the Irpinia fault: Implications for earthquake recurrence in the southern Apennines, Italy, *Journal of Geophysical Research* **98**, 6561–6578.

Seed, H. B., and Idriss, I. M., 1969. Influence of soil conditions on ground motions during earthquakes, *J.Soil Mech. Foundations Div., ASCE* **95**, 99–138.

Vucetic, M., and Dobry, R., 1991. Effects of soil plasticity on cyclic response, *J. Geotech.Eng., ASCE* **117**, 89–107.

Walling, M., Silva, W. J., and Abrahamson, N. A., 2008. Nonlinear site amplification factors for constraining the NGA models, *Earthquake Spectra* **24**, 243–255.

U.S. Geological Survey (USGS), 2003. *Rupture in South-Central Alaska—The Denali Fault Earthquake of 2002*, U.S. Geological Survey Fact Sheet 014-03, available at http://pubs.usgs.gov/fs/2003/fs014-03/.

(Received 6 July 2013; accepted 9 June 2014)